

# An approach to the characterisation of the performance of a tidal stream turbine



Matthew Allmark, Roger Grosvenor, Paul Prickett\*

Cardiff Marine Energy Research Group (CMERG), Cardiff School of Engineering, Cardiff University, Wales, UK

## ARTICLE INFO

### Article history:

Received 14 June 2016

Received in revised form

8 March 2017

Accepted 1 May 2017

Available online 2 May 2017

### Keywords:

Tidal stream turbine

Time-frequency methods

Rotor fault diagnosis

Motor

Generator test bed

## ABSTRACT

In order to better manage and maintain deployed Tidal Stream Turbine (TST) devices their response to complicated and severe loading mechanisms must be established. To aid this process the research presented details a methodology for mapping TST operational data, taken under a variety of operating conditions, to a set of model parameters. The parameter sets were developed based on a TST rotor torque model which, as well as providing means of characterising turbine behaviour, can be used to create TST simulations with minimal computation expense. The use of the model in facilitating parameter surface mapping is demonstrated via its application to a set of rotor torque measurements made of a 1/20th scale TST during flume testing. This model is then deployed to recreate the known rotor behaviour which is compared with the original flume based measurements. This is a flexible tool that can be applied to investigate turbine performance under conditions that cannot be readily replicated using tank-based experiments. Furthermore, Computational Fluid Dynamics simulations of such conditions could be time consuming and computationally expensive. To this end, the use of the model in creating drivetrain test bed based simulations is demonstrated. The model, which can be calculated in real-time, is used to develop representative turbine simulations at high turbulence intensity levels which were not achievable during flume experimentation. The intention is to provide a test-bed for future turbine performance monitoring under more realistic, site specific conditions. The work will also support the deployment of performance surfaces in real-life turbine applications.

© 2017 The Authors. Published by Elsevier Ltd. This is an open access article under the CC BY license (<http://creativecommons.org/licenses/by/4.0/>).

## 1. Introduction

Tidal Stream Turbines (TST) renewable energy devices of commercial scale are currently being designed, deployed and tested. It is known that their operation within hostile marine environments will lead to significant and challenging dynamic loading regimes. The support they require to assure their long term operation in such environments is creating an increasing awareness of the required TST performance management and the associated maintenance activities. To date this work has been very well informed by intensive research and development activity based upon the utilisation of tools such as Computational Fluid Dynamics (CFD). Related research has considered the testing of model scale turbines in as near to realistic flow environments as can be achieved in

flumes and tow tanks. This valuable body of work has been typically used to verify CFD models and as a staging point in the design of full scale TST. There remains a gap however in the replication of conditions to which these devices will be exposed in actual installations.

It is not the intention of this paper to fully review the extensive body of work reported in the above fields. In both cases research undertaken by the Cardiff Marine Energy Research Group (CMERG) is utilised here to support the developments considered here in. In doing so the work provides an additional tool in TST device development which takes the form of a parametric model and drive train simulator test bed. The parametric model and its associated parameter set allow for a standard characterisation of cyclic turbine rotor behaviours. This notion could possibly provide a useful extension to the non-dimensional performance curves commonly utilised to characterise TST operation [2]. The model format seeks to be flexible and to allow for characterisation from a variety of data sources. Furthermore, the model can be used to calculate developed turbine rotor torque in real-time allowing it to be used as input to

\* Corresponding author.

E-mail address: [Prickett@cf.ac.uk](mailto:Prickett@cf.ac.uk) (P. Prickett).

drivetrain test bed simulations. This notion is demonstrated herein. The intention of this simulator is to recreate the results of realistic flow conditions on the TST rotor and apply these as inputs onto a drive train. These can then be used to operate a generator to produce outputs that will provide the basis of TST performance monitoring algorithms. The key concepts utilised in this paper uses outputs acquired from scale model TST tests to construct characteristic surfaces and operate a drive train simulator. Once verified the simulator can then be used to test more extreme and variable flow conditions and directly measure their effect on generator operation and output to enable the monitoring of turbine performance.

Section 2 of this paper briefly reviews previous research in order to underpin the approach adopted in this work. An overview of the turbine model and parameterisation approach is then presented in Section 3. The outputs of the turbine rotor model based on the developed parametric characterisation of flume based measurements are compared with original scale model datasets acquired. This approach is then adapted and deployed in Section 4 to control the operation of a physical drive train test bed. The intention is to enable more challenging turbine performance testing to be conducted quickly and at low cost within a laboratory environment. These simulations are integrated with the physical drive train emulator setup which operates optimal Tip-Speed Ratio ( $\lambda$ ) control. The results of the simulations are then presented in Section 5. The implications of this approach are then discussed, in Section 6, in the context of its application to turbine monitoring. The paper concludes with an assessment of the further development of the approach and consideration of how monitoring approaches can be developed and implemented. This work is proposed to form the basis of on-going research that will consider and apply these techniques.

## 2. Previous research

Previous and current research within the CMERG has established a series of generic TST models [1]. These combine CFD and structural Finite Element Analysis (FEA) to provide Fluid-Structure-Interaction (FSI) based models. Within a structured framework of simulations these have provided non-dimensional power and thrust curves for a variety of TST configurations and flow conditions [2,3]. This work was confirmed experimentally in tests mainly conducted in recirculating flume tanks [4]. This work can be aligned with findings reported by other investigators [5,6] to provide a good basis for future investigations of turbine operational performance. To this end, this and other research has linked CFD directly with full scale turbine operation [6,7,8]. It is worth noting however, that in all cases the modelling effort and time and computing load associated with the CFD approaches outlined are always stated to be considerable.

Taken as a body of work the modelling and simulation of marine and wind turbines can be considered to be broadly based in five areas: resource simulation, simulation of the turbine rotor, drive train simulation, generator control and grid integration simulation. The simulations have been conducted with varying degrees of complexity and coupling depending on the study requirements. In this research the focus is on a data driven simulation approach. This approach allows for both characterisation and subsequently real-time simulation of TST drive train behaviours. There have been a number of previously published approaches to deploying electrical motor and generator performance of marine turbines to support drive train simulations [10–12]. There is also a body of work relating to the application of electrical power output and

characterisation in the similar field of wind turbine drive train simulation from which important features can be drawn [13–15]. The approach, adopted in this paper, is to produce a drive train emulator based on a motor coupled to a generator. This may consider drive characterisation through a gearbox when simulating indirect-drive turbine setups or without a gearbox when simulating direct-drive turbine setups. Similar methodologies and approaches have been previously demonstrated [9,15,16]. This approach affords great flexibility in terms of rotor or drive train input modelling, allowing the simulation of the rotor only or the simulation of other drive shaft components to be fed into the generator [17]. Furthermore the generator control can be simulated with grid integration emulated via hardware or in software.

The key extension afforded by the parametric modelling approach is to facilitate the simulation and evaluation of non-steady-state conditions thereby allowing the development and testing of both steady state and non-steady state turbine operation. This follows from the recognition that in-situ turbine operation will inevitably be non-steady-state as defined by the turbine design, the characteristics of the tidal resource and the effects of wave-current interaction [18,19]. The approach will ultimately support the monitoring of tidal turbines based primarily upon the response of the generator and/or the associated control actions. The actual implementation of the developed approach will of course depend upon the design and configuration of specific devices deployed. However previous research has considered such systems at a generic level with some good effect [11,15,20] and has identified a number of effective approaches [21,22].

## 3. TST rotor model development and parameterisation based on flume tests

The development of a rotor torque model for a specific turbine rotor based on the results of a transient CFD modelling exercise has been previously reported [9]. The model viewed the torque on the turbine drive shaft developed by the rotor as a composite of three blade contributions each deconstructed into a mean component and a fluctuating component. Each of the blade contributions were then summed for a given tip-speed ratio (TSR) " $\lambda$ " and rotor position to give the torque developed by the rotor, at the given position. Such a formulation, whilst incorporating many simplifications, was convenient for two reasons. Firstly, the turbine rotor torque could be appraised simply with knowledge of the turbine characteristic curves, the model parameters and the position of the turbine. Secondly, the process of constructing the model in itself gave insight into the frequency content of the drive shaft torque observed within the CFD models utilised.

In this paper a similar approach was used to produce a more complete rotor model based on parameterisations created utilising acquired flume data. Details of the flume testing campaign undertaken to support this work can be found in Ref. [29]. The model was formed from a mean component based on the turbine characteristic curves, a fluctuation component based on the frequency content of the rotor torque fluctuations measured during flume testing and a stochastic component simulating experimental, measurement and chaotic effects associated with the flume-based experimental setup. The model format was considered to be useful in providing both a means of characterising turbine rotor behaviour under a range of on-coming fluid velocities and  $\lambda$ -values. This information is presented in the form of parametric surfaces. The model format and parameter mapping process undertaken are presented in this section.

Having considered the strength of the previous formation [9]

and the updated requirements of the next generation model formation, the following rotor model was proposed:

$$\tau = \bar{\tau} + \sum_{i=1}^x \bar{\tau} \cdot a_i \cdot \cos(2\pi\theta + p_i) + Z \quad (1)$$

where  $Z$  is a normally distributed strictly stationary random process with mean,  $\mu = 0$  and standard deviation  $\sigma = f(\lambda)$ ;  $x$  is highest harmonic considered in the model;  $a_i$  is the amplitude of fluctuations, scaled by the mean torque, at various harmonics from 1 to  $x$ ;  $p_i$  is the phase angle at various harmonics from 1 to  $x$ ;  $\theta$  is the position of the turbine rotor with  $0^\circ$  defined as where blade 1 is at “top dead centre”. Lastly,  $\bar{\tau}$  is the mean torque developed by the rotor and is given by:

$$\bar{\tau} = C_\tau \cdot \rho \cdot A \cdot R \cdot U_x^2 \quad (2)$$

The formulation of the model in this way required a number of assumptions and further investigation to confirm the structure. The assumptions and requirements are highlighted below and linked with the sections of this paper in which they are addressed:

**Requirement:** the raw flume data required appropriate processing to define the ‘average’ drive train torque fluctuation characteristics. The data and approach used in meeting this requirement is presented in Section 3.1. The deviation of the experimental data from the mean is then considered in Section 3.2.

**Assumption:** in representing the experimental data in concise and useable set of parameters it was assumed that the deviation of the experimental data from the process mean did not change with rotor position.

**Requirement:** the highest harmonic number,  $x$ , considered within the model must be defined such that the fluctuations in rotor torque due to the underlying physical mechanism are adequately captured. This requirement is developed in Section 3.3.

**Requirement:** in such a model to allow for the operation of the turbine over a range of  $\lambda$  from 0 to 7,  $a_i$  and  $p_i$  must be defined over the harmonics  $i$  and the values of  $\lambda$  can then be considered to be represented as surfaces. This requirement is developed Section 3.4.

**Assumption:** in defining such surfaces it is assumed that  $a_i$  and  $p_i$  are not functions of the turbine rotational velocity nor the fluid velocity but only the non-dimensional quantity  $\lambda$  and the turbine position. This assumption is developed Section 3.5.

### 3.1. Model structure relative to the flume testing data

Pre-processing of turbine rotor loading data acquired from flume testing [29] was undertaken using a Time Synchronous Averaging (TSA) approach. The objective of this approach was to acquire and quantify the ‘average’ drive shaft torque fluctuation characteristics under different flow conditions. TSA is utilised extensively in the application of vibration monitoring to rotating machines and has a natural application in this area. The algorithms used are often simple and seek to characterise the underlying transient artefacts in a signal taken from rotational machinery. The general process of TSA can be considered to consist of three phrases: data capture in the time-domain, followed by re-sampling to fixed locations in the displacement domain and averaging over multiple machinery rotations at each (re)sample location. The method of averaging at specific sample points for multiple rotations has the effect of reducing noise in the signal and was used here to highlight underlying characteristic fluctuations over a single turbine rotation. The application of TSA produced an estimate of the underlying torque transients in the data sets observed for differing rotor conditions. The goal of the application was to highlight the average cyclic torque variations

over a single rotation of the turbine.

The data captured during the flume based experimentation was representative of a variety of turbine operating conditions - for various values of  $\lambda$ , composed of differing rotor velocities and fluid velocities. Utilising such data, the torque fluctuations over a turbine rotation were studied for each operating condition; an example of the results of are presented for a  $\lambda$ -value of 3.6 and a flow velocity of  $1 \text{ ms}^{-1}$  in Fig. 1. The information supplied by the data represented in this way formed the, ‘training data’ for the parametric model.

The TSA process was used to capture the average or underlying fluctuations in drive shaft torque as a function of the turbine position. The raw data acquired in this way was then incorporated into the model structure represented in Equation (1). This processes was considered to provide a means of turbine performance characterisation. The drive shaft torque for a given position was represented as a stationary process with mean defined by the first two terms in Equation (1); the distribution about this mean is then given by the standard deviation of the random variable,  $Z$ . This approach is shown conceptually in Fig. 2. The mean value of the process is shown and the Gaussian distribution from which a ‘realisation’ of drive shaft torque is sampled is depicted for the  $240^\circ$  rotor position. The distribution of the process over the turbine position is also represented. It should be noted that the process shown conceptually in Fig. 2 is equivalent to a maximum likelihood fitting of a Gaussian process to the data. This is the case as, for a Gaussian process, the maximum likelihood estimation of the process distribution is given by a Gaussian distribution with the mean given by the mean value of the data and the standard deviation given by the standard deviation of the data [27,28].

The analysis outlined below was applied to data acquired from flume experiments conducted for flow velocities of  $0.9 \text{ ms}^{-1}$ ,  $1.0 \text{ ms}^{-1}$  and  $1.1 \text{ ms}^{-1}$ . Flume data was obtained by testing for the following seven values of  $\lambda$ : 1.5, 2.5, 3.0, 3.5, 4.0, 4.5 and 5.5. In this way parametric surface were developed which creating a characterisation of the turbine operation under a variety of operating conditions.

### 3.2. Standard deviation of the flume data at differing rotational displacements and $\lambda$ -values

To highlight that the Gaussian or Normal distribution was a suitable choice in representing the uncertainty in flume measurements, probability density functions (PDFs) were fitted to the flume data for differing turbine rotational positions. Fig. 3 shows the results of this process for rotor displacements of  $120^\circ$  and  $240^\circ$  for flume tests undertaken at a  $\lambda$  value of 3.6 and fluid velocity of  $1 \text{ ms}^{-1}$ . The structure of the histograms and the fitted probability density functions highlight that the model form chosen - in particular the Gaussian distribution of torsional data at a given rotational displacement - can adequately describe the turbine rotor behaviour.

To finalise this aspect of the mapping of turbine behaviour to the parametric model the effect of the fluid velocity and  $\lambda$  on the variability of the measured rotor torque was studied. These considerations were undertaken to capture the change in the standard deviation of the random variable  $Z$  at differing operational conditions - again the goal was to adequately capture and summarise turbine characteristics in the parametric format afforded by the turbine rotor model. Fig. 4 shows the effect of fluid velocity and  $\lambda$ -value on the observed standard deviation of the measured drive shaft torque. The figure shows that at extreme  $\lambda$  values larger distributions in the rotor torque data were observed. To offer convenience in the model structure a

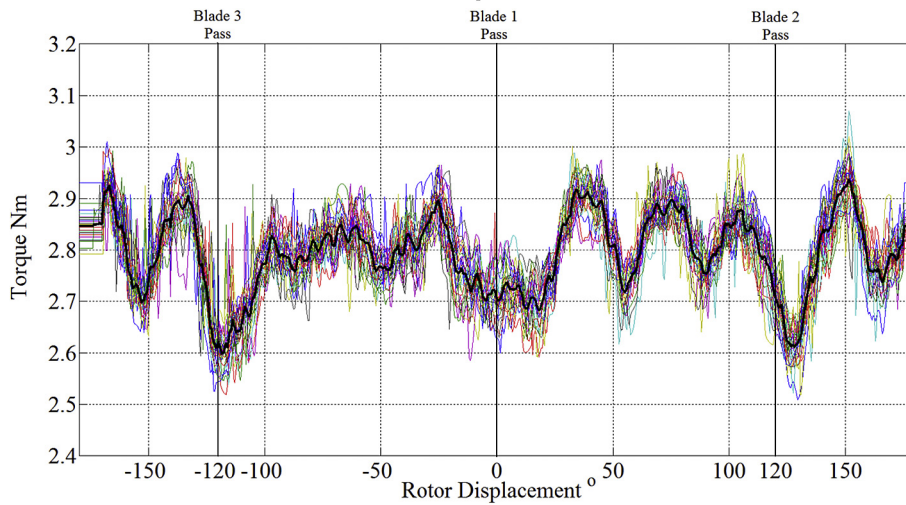


Fig. 1. TSA of the flume data used to parameterise the TST rotor model presented, the case shown is for  $\lambda = 3.6$  and fluid velocity 1 m/s.

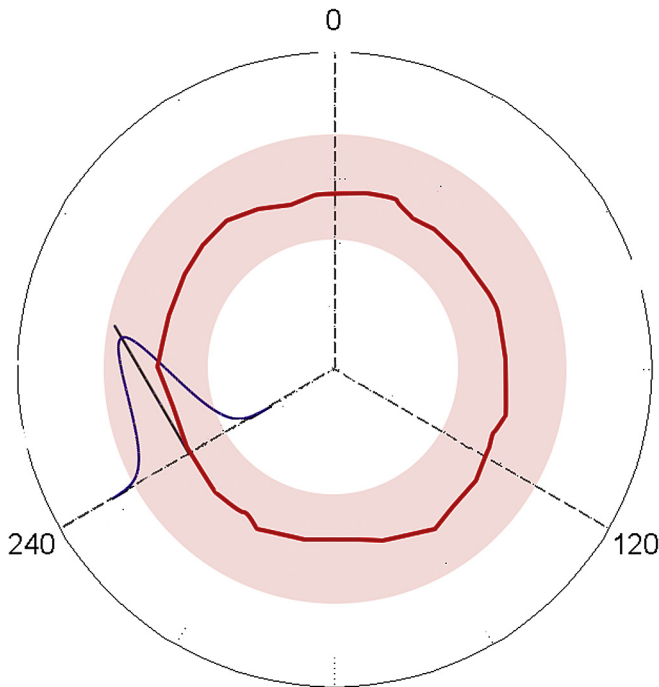
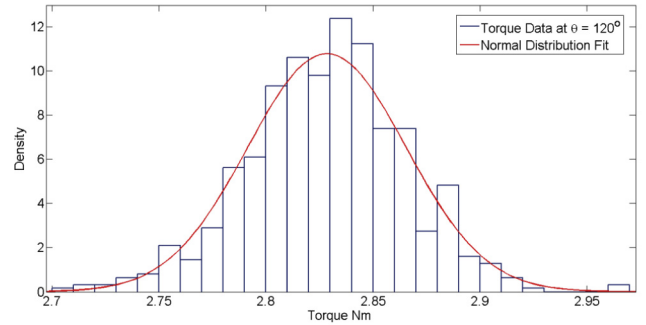


Fig. 2. Schematic representing the model form, highlighting the notion that Equation (1) represents a realisation of a Gaussian process.

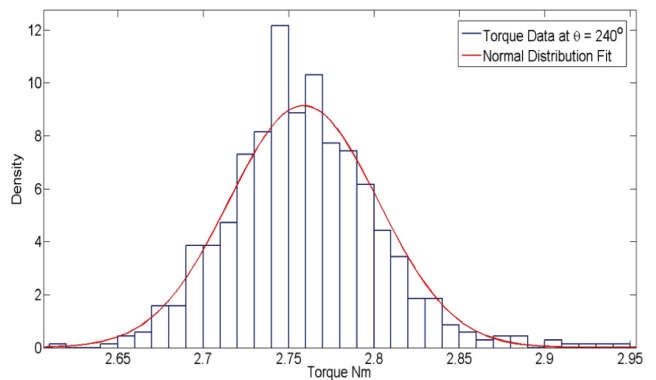
single quadratic function was used to define the change in the standard deviation of the random variable,  $Z$  with  $\lambda$ -value. The quadratic function, which was fitted to the mean of the standard deviations observed for each fluid velocity, is shown in Fig. 4.

### 3.3. Frequency content of the flume data

To further interrogate the data sets, spectrums relating to each condition for both the raw and TSA generated data were produced. This process is represented in Fig. 5 which shows the spectrum of the data presented in Fig. 1. The spectrum of the TSA data and the raw data are compared to confirm no spurious



a)



b)

Fig. 3. Histograms showing the Gaussian or normal distribution of the capture flume data for a given turbine position.

artefacts were introduced via the processing method. The frequency axis of each spectrum was normalised by the mean turbine rotational velocity for each given dataset. The frequency content is thus presented in-terms of the harmonics of the rotational frequency of the turbine.

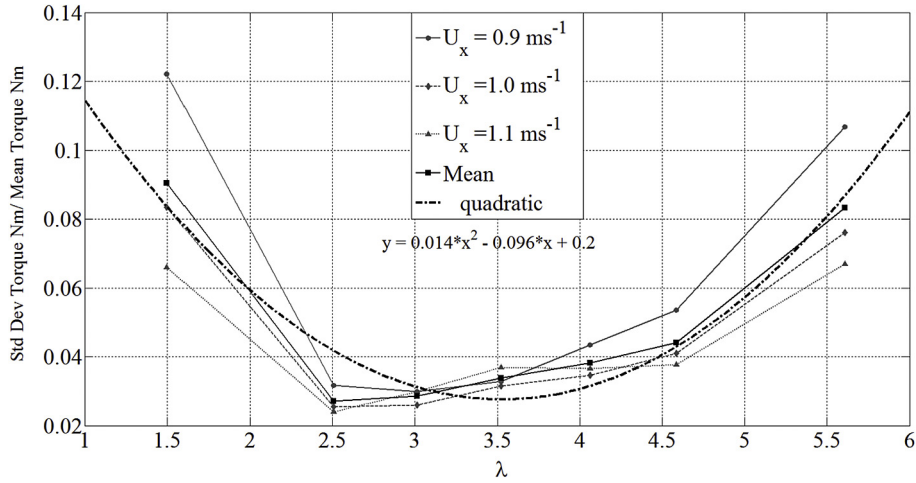


Fig. 4. Figure showing the effect of Lambda and oncoming fluid velocity on the spread of the experimental data. A quadratic function has been fitted to the mean standard deviations from each fluid velocity case.

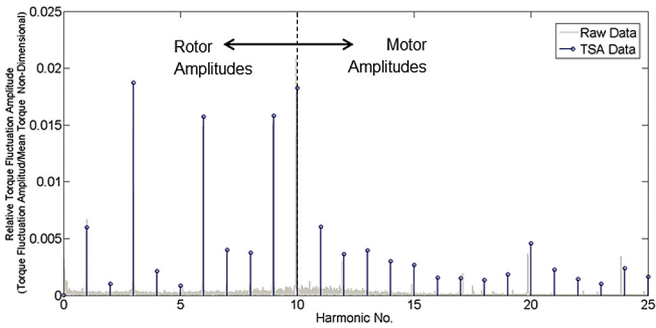


Fig. 5. Amplitude spectrum of the drive shaft torque for the optimum rotor setting with a flow velocity of 1 ms<sup>-1</sup>.

In terms of the prominent amplitudes observed in the two spectrums, harmonic numbers 1, 3, 6, 9 and 10 show the greatest contribution to drive shaft torque fluctuations, relative to the mean torque. To parameterise the model effectively it was required that the model should only consider harmonics that relate to torque fluctuations resultant from fluid-rotor interaction. Specifically, harmonic amplitudes relating to the permanent magnet synchronous motor (PMSM) and the drive shaft bearings needed to be filtered or reduced to provide a more satisfactory rotor torque parametric model.

The amplitudes relating to the 3rd and 6th harmonics of the rotational velocity of the turbine were considered to arise from the so-called shadowing effect. The shadowing effect is observed as turbine blades pass the turbine stanchion and are characterised by a drop in the developed rotor torque at such displacements – in this case at 0°, 120° and 240°. The smaller amplitude observed at the 1st harmonic of the rotational frequency of the turbine was considered to be a result of imbalance in the turbine setup. As care was taken during flume testing to minimise any imbalance in the rotor setup the amplitude of the 1st harmonic relative to the 3rd and 6th harmonics is significantly smaller in magnitude. Indeed, greater rotor imbalance has been shown to increase the amplitude of the 1st rotational harmonic. This notion has been exploited in previous research as the basis of a TST rotor imbalance monitoring system [9].

Based upon known turbine characteristics it was considered

that the 9th and 10th harmonic amplitudes were due to the pole passing frequency associated with the PMSM which had 10 pole pairs. This was further confirmed by the peak evident at the 20th harmonic. This allowed the assertion that no significant harmonics were present passed the eighth harmonic in the overall torque spectrum shown. This decision has been highlighted in Fig. 3 where the distinction between the lower frequency rotor artefacts and the higher frequency motor artefacts is highlighted.

From this and similar analysis of the other flow condition results it was considered that the TSA processed data suitably represented frequency domain characteristics of the measured rotor torque during the flume testing campaign. This confirmed that the TSA data provides an accurate representation of the turbine characteristics and can therefore be used as parameterisation data in further developments.

### 3.4. Parameter surface development

A set of spectrums, similar to the one shown in Fig. 5, were calculated for each of the  $\lambda$  values. The amplitudes were scaled by the average torque,  $\bar{\tau}$ , developed for the given operating condition. Surfaces were then developed by inputting the known relative amplitudes and phase angles, at the eight harmonics and seven  $\lambda$  values measured in the flume experimentation, into a 3-dimensional array. A curve fitting applet was used to construct each surface using a Bi-Harmonic Spline interpolation. The 56 data points used in this process are visible as black dots in Figs. 6 and 7. In the case of the phase surface fit the phases were ‘unfolded’ empirically to minimise spurious surface gradients which arose from the phases being close to the  $-180^\circ$  and  $180^\circ$  boundaries. It was observed that a similar surface structure was found for both relative amplitude and phase surface for the 0.9, 1.0 and 1.1 ms<sup>-1</sup> flow velocities considered. It is noted that future users of this process should carefully consider the performance of the interpolation scheme used. This could be improved by generating more data during experimentation and dividing the data into, ‘training’ data and ‘test’ data. A variety of processes for fitting functions to the data or interpolating between data points exist - such as, regression [32], Kriging [33] and linear interpolation.

An important feature apparent in the developed surfaces was the increase in relative amplitude for the 1st, 3rd and 6th harmonics corresponding with increasing values of  $\lambda$ . Importantly, this

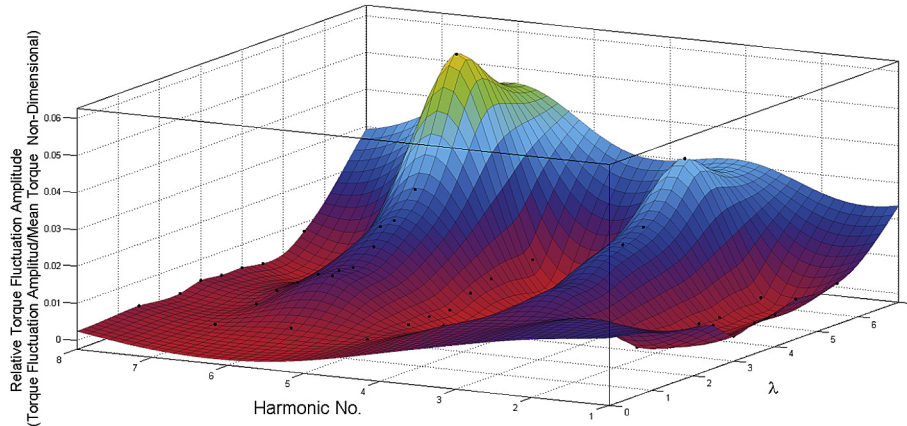


Fig. 6. Amplitude surface generated for a  $1 \text{ ms}^{-1}$  fluid velocity and optimum rotor condition.

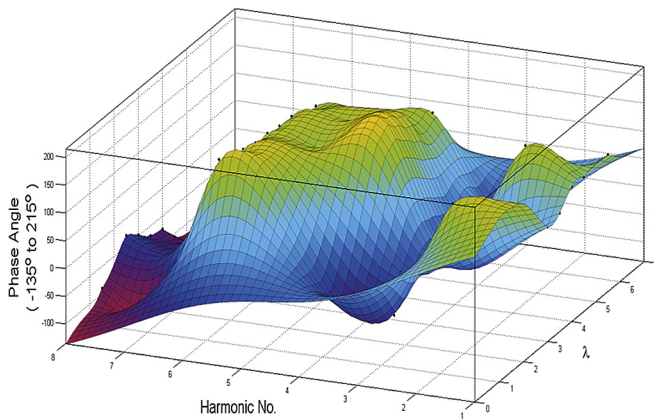


Fig. 7. Phase surface generated for a  $1 \text{ ms}^{-1}$  fluid velocity and optimum rotor condition.

variation in spectrum structure with  $\lambda$  is well captured by the model and associated parameter sets. This could well provide a ‘transient benchmark’ for monitoring activities or could be used, as is demonstrated in Section 4, to create drive train simulations which included this complex change in torque structure as a function of  $\lambda$ .

3.5. Torque frequency characteristics vs tip-speed-ratio

In this section consideration is given to the suitability of the developed surfaces to represent turbine operation under varying fluid velocities. To verify that the rotor model under development could be represented using these surfaces the relative amplitude and phase spectrums were plotted for each value of  $\lambda$  for the three fluid velocity values tested within the flume testing campaign.

It is clear that the relative amplitude spectrums, shown in Fig. 8 for each of the three fluid velocities (0.9 m/s, 1.0 m/s and 1.1 m/s), are in generally good agreement. The exception is the spectrum observed for  $\lambda$  equal to 1.5. This suggests that for  $\lambda$  values above 1.5 the relative drive train torque fluctuations are a function of the non-dimensional quantity and not the specific flow speed and rotational velocity used to calculate said non-dimensional value. Therefore, the rotor torque simulation method proposed can be utilised for variable speed turbine operation, if limited to operation above a  $\lambda$

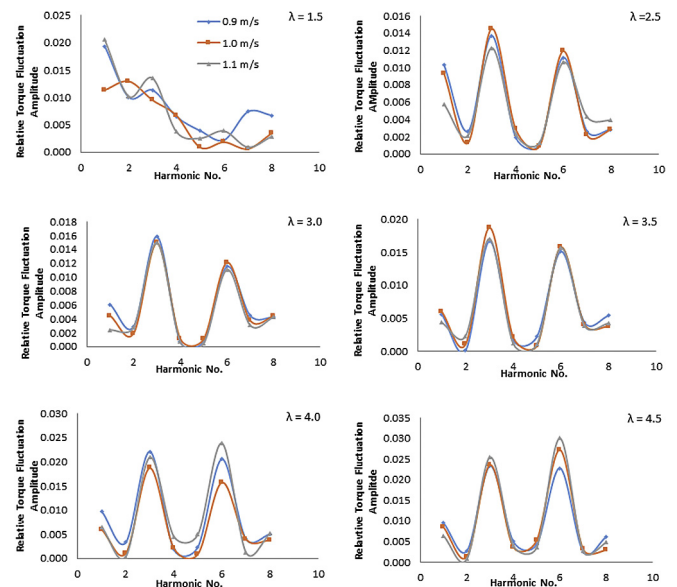


Fig. 8. The Amplitude spectrum of the 1/20th scale turbine driveshaft torque at varying tip-speed-ratios.

value of 1.5. This restriction, it should be noted, was considered to have little impact on the proposed simulations as, due to the optimal  $\lambda$  control schemes utilised, the operating range of  $\lambda$  expected would be,  $2 < \lambda < 4$ .

The phase spectrums generated for the same conditions are shown in Fig. 9. This seems to present an altogether more complicated relationship over the  $\lambda$  values studied. There does seem to be agreement between the phase spectrums for  $\lambda$  greater than 3.5. Furthermore, it is worthwhile noting that the phase angles are consistent and in good agreement for the 1st, 3rd and 6th harmonics. Specifically, it was observed that the 1st harmonic occurs between the 70° and 90° phase angles. Values of between 350° (−170°) and 380° (+160°) were generally observed for the 3rd harmonic and phase values of between 150° and 180° were observed for the 6th harmonic. As such it was considered suitable to engineer a single surface structure for the range of fluid velocities utilised in the simulations.

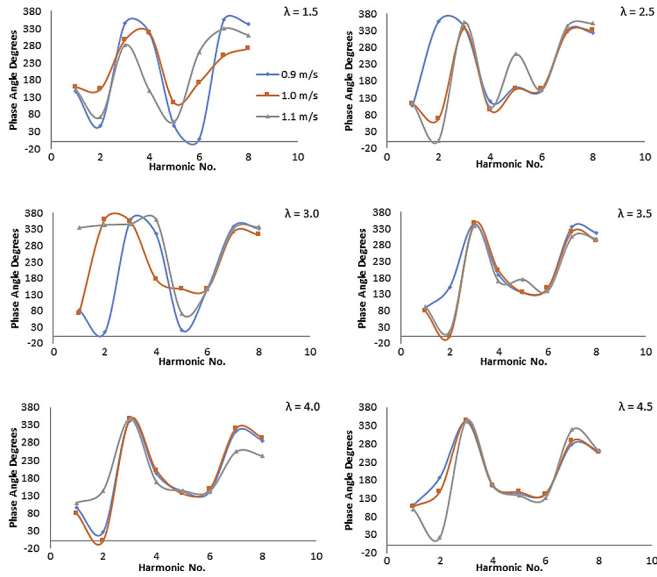


Fig. 9. The phase spectrum of the 1/20th scale turbine driveshaft torque at varying tip-speed-ratios.

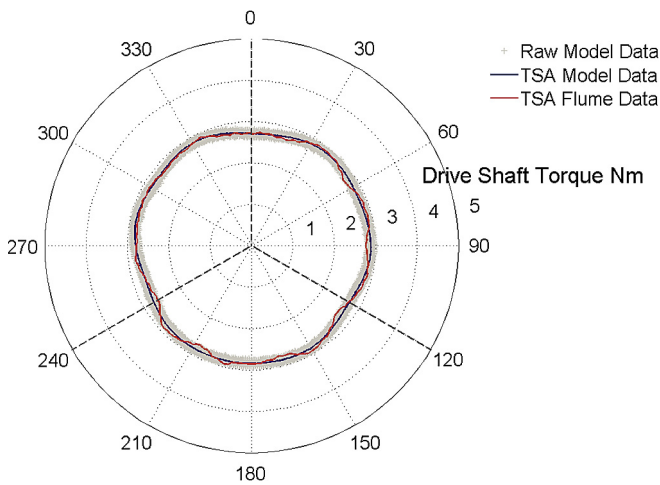


Fig. 10. Comparison of the flume data, both raw and processed, with the parametric rotor model output.

### 3.6. Comparison of flume data and model output

To show the effectiveness of the parametric model and associated parameter mapping process to represent the turbine rotor performance observed during flume testing the model output was calculated for the known operating conditions undertaken during the flume experimental campaign. Fig. 10 shows a comparison between the flume data used to parameterise the turbine model and the output of the turbine model. It can be seen that the two are in good agreement, this was observed for all test cases considered. The authors note that, although generally good agreement between the model and flume data was observed, a discrepancy between the model and the data at higher frequencies was found. This can be seen in Fig. 10 by the periodic fluctuations in the flume data which are not present in the model data. This was expected as, following on from discussion in Section 3.3 and as shown in Fig. 5, these higher frequency fluctuations were considered to be related to the

pole passing frequency of the PMSM used to make the torsional measurements. As such it was considered that these discrepancies were a direct result of the decision to suppress these frequencies in the parametric model. Furthermore, it is noted that these could easily be captured by extending the range of harmonics for the model was parameterised. It was seen by the authors that this ability to map model parameters based on harmonics of interested was a strength of the model format and parameterisation process outlined.

## 4. Drive train test bed implementations

To illustrate a potential use of the parametric model formulation outlined in Section 3, the model parameterised based on the flume-scale measurements was used to create hardware-in-the-loop simulations. To further demonstrate the flexibility of the model format simulations were created relating to non-steady state turbine operation. Specifically, Non-steady state simulations were developed for 10% turbulence intensity fluid velocity input along with an optimal  $\lambda$  turbine control scheme.

Fig. 11 provides an overview of the simulation structure developed. The aim was to allow the appraisal of turbine rotor torque at differing rotor displacements under a wide range of operating conditions. It was set up to use a one-dimensional stochastic fluid velocity model. The dynamic effects of tip-speed ratio based control to maintain the optimum power production operational conditions were also included. The structure underpins the ability to observe and test differing TST operating scenarios using a physical drive train test bed. A full overview of the LabVIEW software produced to undertake the simulations can be found in Ref. [29].

### 4.1. Hardware set-up

Fig. 12 shows the drive train test bed developed for tidal stream turbine simulations. The test bed motor can be controlled to replicate the turbine rotor input to the drive train. In this case the motor is directly coupled to a generator for power extraction thereby effectively enabling the simulation of both a direct-drive and geared tidal stream turbine equipped with a permanent magnet synchronous generator. A proprietary flexible coupling was used to connect the machine’s drive shafts. To allow for variations during future testing the two rotating machines were mounted on a rail allowing the separation between them to be increased so that gearboxes and other drive shaft components could be included in the test bed. The two rotating machines are of the servo type with on board encoders measuring the rotor velocity and position for feedback control.

The two motor/generators shown in Fig. 12 were set-up to operate as master and slave. The master drive was connected via Modbus TCP/IP to a National Instruments Compact RIO. The TST model and maximum power point tracking control loops were implemented using a real-time operating system in the Compact RIO. The motor drives utilised close-loop vector oriented control to implement the commands sent from the Compact RIO. This set-up utilised a microprocessor for implementing control algorithms. It also enabled data streaming via a set of field-programmable gate array connected reconfigurable input/output modules. The controller Ethernet chassis enabled it to be directly connected to a PC. The TST model and maximum power point tracking control loops were implemented using a real-time operating system within the controller and the rotor and generator commands were sent to the motor drives via the Modbus link. The motor drives utilised close-loop vector oriented control to implement the commands sent from the controller.

For the simulations undertaken the speed of the turbine was set

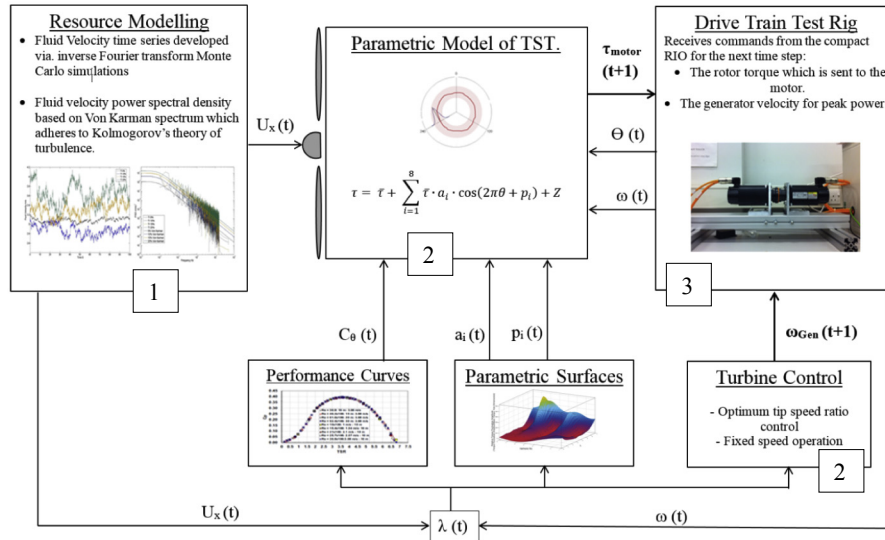


Fig. 11. Overview of the simulation process based on the parametric form outlined throughout Section 3.

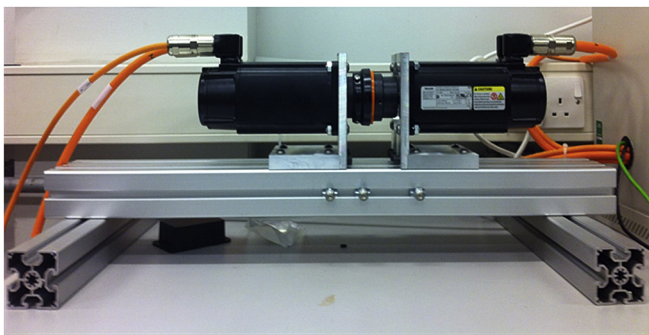


Fig. 12. The drive train test bed utilised for scale turbine drive train simulations.

simulation calculations and the storing of data for further analysis. The numbers circled within each of the elements relate the elements of the overall simulation schematic presented in Fig. 11 to the hardware. Specifically the calculation of each numbered element is undertaken via the hardware labelled with the corresponding number in Fig. 13.

4.2. Drive train operation of turbine control

To simulate turbine dynamics in a more rigorous and representative manner variable speed turbine control was also developed for the experimental simulations. This was included to allow for intended condition monitoring functions to be developed and tested based on the simulation results. The variable speed turbine control scheme used was that of optimal tip-speed ratio. The method involved taking fluid velocity and turbine rotational velocity measurements required to define the turbine operating tip speed ratio. The measured operating point was compared with a set-point tip speed ratio, known prior to operation to give maximum power output under continuous turbine operation. The error value was passed to a controller to regulate the generator load to achieve the torque required to minimise the tip speed ratio error. During the experimental simulations, the torque set point command was input to the motor drive used and the internal control structure was used to control the drive.

4.3. Fluid velocity simulation

The simulations outlined in this paper used the initial assumption that the turbine is subjected to plug flow (spatially uniform flow) conditions. This in effect assumed that the flow velocity in the region of most interest, across the swept area of the turbine, was constant. If found to be significant this step can be modified later to incorporate more realistic and site specific flow conditions. This approach has been shown to have merit [23]. At this stage this simplification was made to align this work with the flow condition set for the CFD models and the approximate conditions for the flume testing. The plug flow assumption leads to a convenient representation of the flow conditions at the turbine rotor. The flow is represented by:

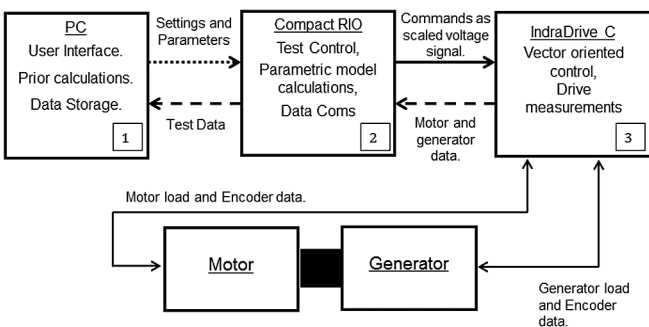


Fig. 13. Schematic of the interacting hardware elements and the distribution of functionalities across the hardware platforms.

by commanding the rotational velocity of the generator which was achieved via load output regulation. The motor was controlled to replicate torque commands output from the parametric model given the current parameters and simulation data. Fig. 13 shows a schematic of the test bed indicating the interaction between each of the hardware elements. The figure also shows the flow of information highlighting the use of measured data for recursive

$$U_x(t) = \bar{U}_x + u'_x(t) \quad (3)$$

where  $U_x(t)$  is the fluid velocity at time  $t$  decomposed into a stationary mean fluid velocity  $\bar{U}_x$  and a fluctuating component  $u'_x(t)$  which is time varying with the  $x$  direction perpendicular to the turbine rotor plane. A natural approach to representing the fluid flow given by the above is to model the fluid velocity fluctuations as a stationary process with given power spectral density characteristics. From Kolomogrov's theory of turbulence [24] the amplitude of the power spectrum should be proportional to  $f^{-5/3}$  as  $f \rightarrow \infty$ , where  $f$  is frequency in Hz. Previous application of the von Karman spectrum [25] for reliability simulations has shown that the above condition can be written in the non-dimensional form:

$$\frac{fS_u(f)}{\sigma_u^2} = \frac{\frac{4L}{U_x}}{\left[1 + 70.78 \left(\frac{fL}{U_x}\right)^2\right]^{5/6}} \quad (4)$$

where  $S_u(f)$  is the spectral density function for the process,  $L$  is the length scale,  $\sigma_u$  is the standard deviation of the process  $u'(t)$ . Note that the "x" subscript is omitted as the formulation outlined here relates to a one-dimensional simulation.

The associated length scale of the turbulent process,  $L$ , for channel flows was assumed to be approximately equal to 0.8 of the channel depth. In this case  $L$  was set to 0.64 m. The standard deviation for the turbulent process is commonly normalised by the mean flow and is named the turbulence intensity. For flows greater than 1.5 m/s the expected range of turbulence intensities is between 0.05 and 0.1 [26]. Here turbulence intensity is given by:

$$I_U = \frac{\sigma_u}{U_x} \quad (5)$$

A detailed outline of the calculation procedure can be found in Ref. [29].

## 5. Initial drive train test bed results

This section provides an overview of the results obtained from the drive train emulator simulations. The output from both the motor and the generator was then captured in real time. The outputs from each of these fluid velocity simulations developed were

150 s in length.

Fig. 14 shows one realisation taken from the test case set of twenty fluid velocity simulations created to test the initial stages of the modelling approach. In this case this series of tests had a set mean fluid velocity of  $1 \text{ ms}^{-1}$  and a set turbulence intensity of 10%. The 150 s data set is seen to exhibit realistic variations in velocity around this mean with the effect of this (most extreme) turbulence intensity being clear. This was to be deployed to simulate rotor operation and form the input into the drive train test bed. The observed power spectra for the data is shown in Fig. 15 highlighting the adherence to the Von-Karman spectra discussed in section 4.3.

Fig. 16 depicts the results of non-steady state simulations with the inclusion of the turbulent fluid velocity time series discussed in the tidal resource simulation model outlined in Section 3.1. Accordingly, it can be seen that fluid velocity fluctuations are included in the simulations and as a result of the optimal TSR control scheme adopted rotational velocity fluctuations of the turbine can also be seen. Furthermore, due to the change in fluid velocity additional fluctuations can be seen in the torsional input of the motor. These additional fluctuations are also evident in traces for power output and quadrature axis current measured via the generator PMSM control system.

## 6. Discussion

The paper outlines a parametric model format and the associated parameterisation process. The parameterisation process could well allow researchers and device developers to approach transient torque loading in a consistent and structured manner. Indeed, a number of conclusions and insights were afforded as a result of the parameter mapping process. Whilst the goal of the model format was to allow for flexibility and complexity during turbine characterisation, further research is required to verify that the model structure and parameter mapping process allow this under more realistic turbine operating conditions. This limitation to the research was resultant from the format of the flume testing data utilised in this instance. The model and parameterisation process are on-going areas of research and it is the goal of the researchers to test the validity of the approach utilising data captured under more realistic flow conditions. Furthermore, to increase the understanding and knowledge of the suitable application of this process, the researchers hope to test its

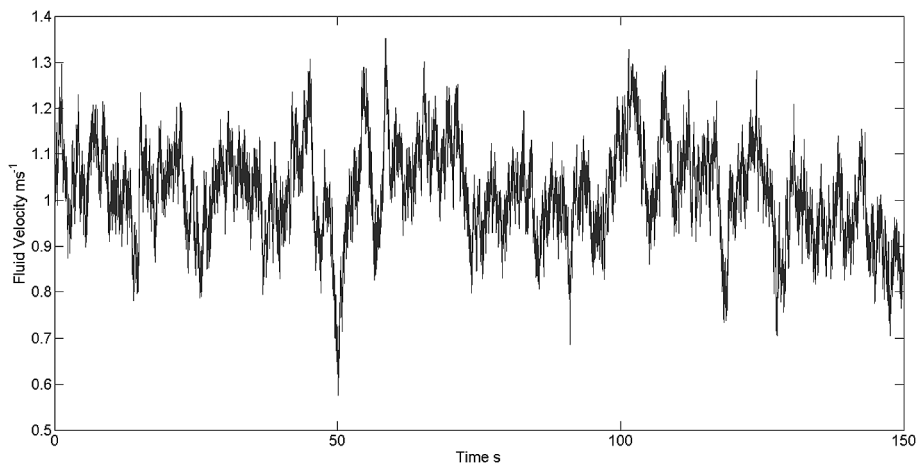


Fig. 14. Example of the drive train test bed rotor generated fluid velocity time series.

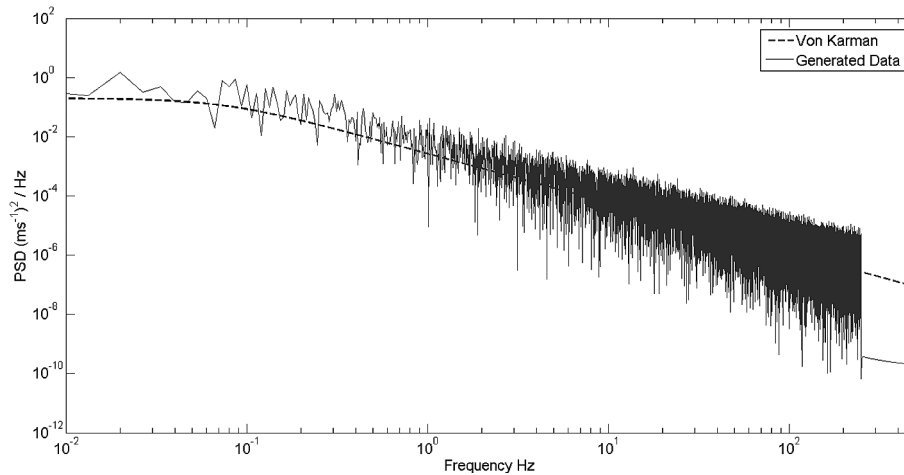


Fig. 15. Comparison of the von Karman spectrum and the spectrum observed for the single instance time series shown in Fig. 10.

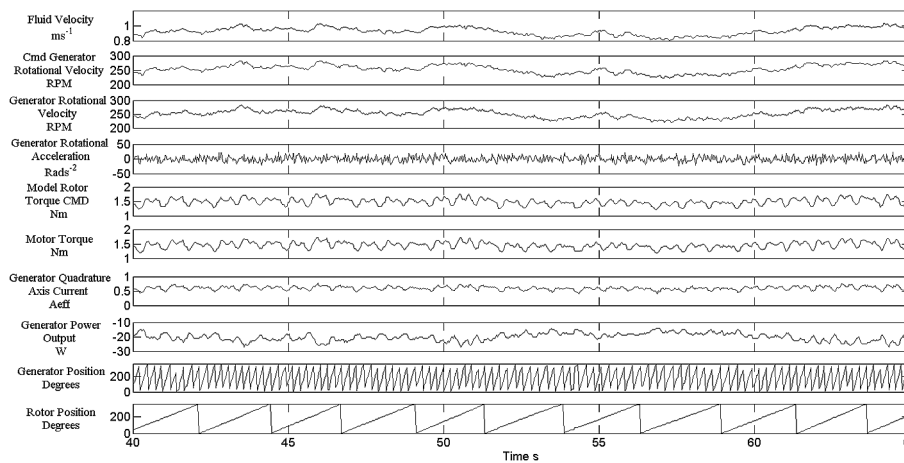


Fig. 16. The results from a real-time drive train simulation of the optimum rotor case with Turbulence Intensity = 10%.

applicability on a variety of rotor setups utilising differing blade profiles and rotor diameters. A potential method for creating turbulence of known characteristics within flume testing has been reported by Blackmoore et al. [30]. Furthermore, wave/current interaction testing has been outlined by Ordonez et al. [31]. These approaches to flume and tow tank testing respectively could well be utilised in future test campaigns to provide more realistic operational data.

The approach in this initial investigation, into the use of the parametric model as input to a drive train test bed, used a one-dimensional stochastic fluid velocity model. This was manipulated to output the fluid velocity time series which exhibited von Karman spectral properties. The approach was designed to allow for the incorporation of more realistic flow regimes in the future. This is the subject of on-going work [23] and the incorporation was allowed for in the parametric model based design approach. It must be stressed that this was a design attribute meaning that site-specific flow conditions can be input into this simulation technique, allowing for enhanced turbine performance modelling pre-installation and supporting post-installation performance monitoring and management.

In terms of the impact of this work on the research community it can be asserted that the developed approach can be further developed and adapted to simulate a variety of different operating conditions. The surfaces used for parameter lookup can be extended to include transients introduced by differing drive train sub-assemblies. In this way, the non-steady state simulation approach can be utilised going forward in a number of useful ways including the simulation of bearing and gearbox fault conditions. The approach was also intended to enable further research exploring the turbine's response to specific fault condition scenarios. In doing so it was a defined objective to engineer the developed simulation so it could also be extended to incorporate a number of differing rotor fault conditions. The intention was to enable the development of the surface generation process to support condition monitoring procedures by considering the distortion of the monitoring surfaces under anomalous rotor condition relative to the generated surface for optimal rotor conditions. As such the system developed was intended to form an integrated fault simulation test bench which has been subsequently utilised for the testing and development of a number of differing TST condition monitoring approaches. The results of this condition monitoring

system research will be provided in a future publication aligned with this paper.

## 7. Conclusions

A parametric model of the torque developed via a TST rotor, and experienced by a TST drive train, has been outlined. The process of parameterising the model has also been detailed and it was shown that the model form adequately captured the mean, cyclic and stochastic torsional loading inputs.

In undertaking the parametrisation of the turbine model time-synchronous averaging was successfully utilised to define the underlying cyclic variations observed in the torque developed via the TST rotor. The process was shown to be suitable and, indeed, normal distribution of torque data was observed at differing rotor displacements. Furthermore, considerations of the frequency domain characteristics of the TSA data and raw data showed that the TSA process does not adversely affect frequency domain representations of the rotor torque developed. The cyclic nature of the rotor torque highlighted via the TSA processing was captured in the parametric model via a Fourier series.

The stochastic nature of the data was captured in the model by a random variable  $Z$ . This random variable had mean of zero and a standard deviation defined by the standard deviation of the data. It was assumed that the standard deviation was constant with respect to turbine displacement. It was found that the standard deviation of the rotor torque, relative to the mean rotor torque, exhibited approximately quadratic properties with respect to  $\lambda$ . The quadratic minimum was found to be in the range of  $2.5 < \lambda < 3.6$ . Increase spread in the data relative to the mean value was observed for the stall and freewheeling regions – for  $\lambda < 2.5$  and  $\lambda > 5$ .

Parametric surfaces were developed capturing the complex variation the amplitude of harmonic torque fluctuations with  $\lambda$ . The amplitude surface shows that a relative increase in torque oscillations can be observed for higher value of  $\lambda$ . The phase surface shows consistence between 4th and 6th harmonics for  $2 < \lambda < 5$ , the phase angle observed is in the region of  $180^\circ \pm 20^\circ$ . Phase angles in vicinity of the  $90^\circ$  were found for the 1st harmonic and in region of  $360^\circ$  or  $0^\circ$  for the 3rd harmonic. These findings were reasonably consistent for the three fluid velocity settings tested.

The authors note that Bi-Harmonic Spline interpolation was used to illustrate the overall mapping process developed

throughout the paper and would like to highlight a number of caveats. Specifically, care should be taken by researchers looking to use or develop this method to check that a suitable surface fitting or interpolation scheme has been used. This requires using experimental data that has not been used in generating the model to check the accuracy of the surface between the data points used for construction. As was the case with the drive train simulations presented the user should avoid using data outside of the convex hull of the ‘training’ data as extrapolation beyond this range leads to high uncertainties in the model output.

The model was used as an input to a drive train test bed simulation apparatus. In order to integrate the model into the test bed real-time calculation of the model was required and demonstrated. The model took as input simulated fluid velocities of mean  $1 \text{ ms}^{-1}$  and TI of 10%. The test rig utilised optimal  $\lambda$  control.

## Acknowledgements

The authors acknowledge the financial support of EPSRC EP/J010200/1 under the Supergen Marine Grand Challenge programme.

## Appendices

### A. Steady State Drive Train Simulations:

To confirm the correct operation of the drive train test bed and parametric model setup outlined in Section 4, steady state simulations were undertaken. The simulation used as input the parameter set developed throughout Section 3, a fixed on coming fluid velocity of  $1 \text{ ms}^{-1}$  and a fixed  $\lambda$  value of 3.5. The correct operation of the turbine rotor model, utilising the generator position and velocity measurement feedback, was confirmed by viewing the spectrums input via the amplitude surfaces utilised for the model calculation. These spectrums were compared with the spectrums observed for the motor torque command value and the achieved motor input torque values. Fig. 17 shows the model amplitude parameters during the steady-state simulations. Fig. 17 also shows the spectrums observed at the model output and measured via the motor feedback system. The agreement of the three spectrums plotted in Fig. 17 confirm the hardware-in-the-loop simulations were operating as expected.

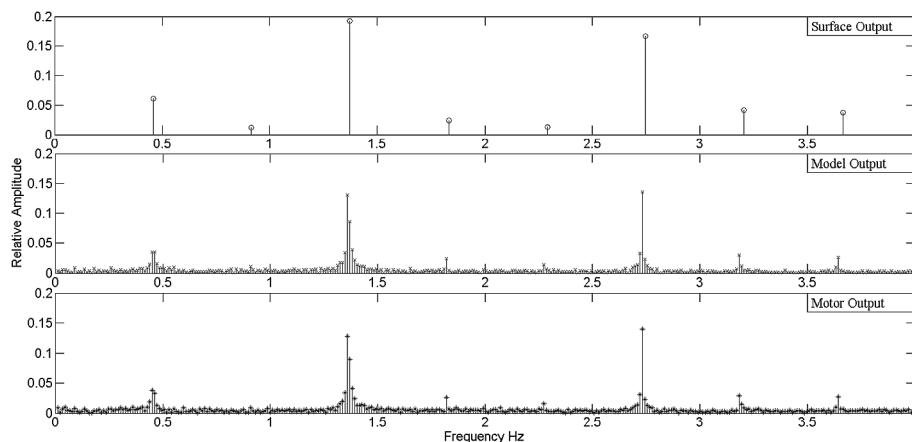


Fig. 17. Model amplitude parameters input for the optimum rotor setting.

## References

- [1] T. O'Doherty, A. Mason-Jones, D.M. O'Doherty, P.S. Evans, C.F. Woolridge, I. Fryett, Considerations of a horizontal axis tidal turbine, *Proc. ICE Energy 163* (3) (2010) 119–130.
- [2] A. Mason-Jones, D.M. O'Doherty, C.E. Morris, T. O'Doherty, C.B. Byrne, P.W. Prickett, R.I. Grosvenor, I. Owen, S. Tedds, R.J. Poole, Non-dimensional scaling of tidal stream turbines, *Energy* 44 (1) (2012) 820–829.
- [3] D.M. O'Doherty, A. Mason-Jones, T. O'Doherty, C.B. Byrne, I. Owen, Y.X. Wang, Experimental and computational analysis of a model horizontal axis tidal turbine, in: 8th European Wave and Tidal Energy (EWTEC 2009), 2009.
- [4] S.C. Tedds, I. Owen, R.J. Poole, Near-wake characteristics of a model horizontal axis tidal stream turbine, *J. Renew. Energy* 63 (2014) 222–235.
- [5] R. McSherry, J. Grimwade, I. Jones, S. Mathias, A. Wells, A. Mateus, 3D CFD modelling of tidal turbine performance with validation against laboratory experiments, in: 9th European Wave and Tidal Energy Conference (EWTEC 2010), 2011.
- [6] I. Afgan, J. McNaughton, S. Rolfo, D.D. Apsley, T. Stallard, P. Stansby, Turbulent flow and loading on a tidal stream turbine by LES and RANS, *Int. J. Heat Fluid Flow* 43 (2013) 96–108.
- [7] J. McNaughton, S. Rolfo, D. Apsley, T. Stallard, P. Stansby, CFD power and load prediction on a 1MW tidal stream turbine with typical velocity profiles from the EMEC test site, in: 10th European Wave and Tidal Energy Conference (EWTEC 2013), 2013.
- [8] A. Mason-Jones, D.M. O'Doherty, C.E. Morris, T. O'Doherty, Influence of a velocity profile and support structure on tidal stream turbine performance, *J. Renew. Energy* 52 (2013) 23–30.
- [9] M.J. Allmark, P.W. Prickett, C. Frost, R.I. Grosvenor, Tidal Stream Turbine blade fault diagnosis using time-frequency analyses, in: 11th European Wave and Tidal Energy Conference (EWTEC2015), 2015.
- [10] G. Caraiman, C. Nichita, V. Minzu, B. Dakyo, C.H. Jo, Real time marine current turbine emulator: design, development and control strategies, in: 20th International Conference on Electrical Machines (ICEM), 2012.
- [11] L. Peretti, V. Sarkimaki, Mechanical drive train emulation by means of electrical drives – a generalised approach, in: 38th Conference of the IEEE Industrial Electronics Society (IECON 2012), 2012.
- [12] L. Sinopoli, M. Ordonez, J. Quaicoe, DSP-based marine current turbine emulator using a 3-phase inverter, in: IEEE Energy Conversion Congress and Exposition (ECCE), 2012.
- [13] S.J. Watson, B.J. Xiang, W. Yang, P.J. Tavner, C.J. Crabtree, Condition monitoring of the power output of wind turbine generators using wavelets, *IEEE Trans. Energy Convers.* 25 (2010) 715–721.
- [14] W. Yang, Condition monitoring the drive train of a direct drive permanent magnet wind turbine using generator electrical signals, *J. Sol. Energy Eng.* 136 (2) (2014) 021008.
- [15] W. Yang, P.J. Tavner, R. Court, An online technique for condition monitoring the induction generators used in wind and marine turbines, *Mech. Syst. Signal Process.* 38 (1) (2013) 103–112.
- [16] A. Bielecki, T. Barszcz, M. Wójcik, Modelling of a chaotic load of wind turbines drivetrain, *Mech. Syst. Signal Process.* 54–55 (2015) 491–505.
- [17] L. Myers, A.S. Bahaj, Power output performance characteristics of a horizontal axis marine current turbine, *J. Renew. Energy* 31 (2) (2006) 197–208.
- [18] A.L. Amarante Mesquita, F.C. Palheta, J.R. Pinheiro Vaz, M.V. Girão de Morais, C. Gonçalves, A methodology for the transient behaviour of horizontal axis hydrokinetic turbines, *Energy Convers. Manag.* 87 (2014) 1261–1268.
- [19] S. Benelghali, M.E.H. Benbouzid, J.F. Charpentier, Generator systems for marine current turbine applications: a comparative study, *IEEE J. Ocean. Eng.* 37 (2012) 554–563.
- [20] W. Yang, P.J. Tavner, M. Wilkinson, Condition monitoring and fault diagnosis of a wind turbine with a synchronous generator using wavelet transforms, in: 4th IET Conference on Power Electronics, Machines and Drives (PEMD 2008), 2008.
- [21] L.F. Villa, A. Reñones, J.R. Perán, L.J. de Miguel, Statistical fault diagnosis based on vibration analysis for gear test-bench under non-stationary conditions of speed and load, *Mech. Syst. Signal Process.* 29 (2012) 436–446.
- [22] M.N. Zaggout, P.J. Tavner, L. Ran, Wind turbine condition monitoring using generator control loop signals, in: 6th IET International Conference on Power Electronics, Machines and Drives (PEMD 2012), 2012.
- [23] S. Tatum, M. Allmark, C. Frost, D. O'Doherty, A. Mason-Jones, T. O'Doherty, CFD modelling of a tidal stream turbine subjected to profiled flow and surface gravity waves, *Int. J. Mar. Energy* 14 (2016) 161–179.
- [24] J.C.R. Hunt, O.M. Phillips, D. Williams (Eds.), *Turbulence and Stochastic Processes: Kolmogorov's Ideas 50 Years on*, Proc. Roy. Soc. London, vol. 434, 1991, pp. 1–240.
- [25] V. Dimitri, D.V. Vala, L. Cherninb, D.V. Yurchenkoc, Reliability analysis of rotor blades of tidal stream turbines, *Reliab. Eng. Syst. Saf.* 121 (1) (2014) 26–33.
- [26] J. Thomson, B. Polagye, M. Richmond, V. Durgesh, *Quantifying Turbulence for Tidal Power Applications*, 2010. OCEANS 2010.
- [27] M. Grigoriu, *Stochastic mechanics*, *Int. J. Solids Struct.* 37 (1–2) (2000) 197–214.
- [28] C.M. Bishop, *Pattern Recognition, Machine Learning*, Springer Science+Business Media, New York, 2006, pp. 78–90.
- [29] M. Allmark, *Condition Monitoring and Fault Detection of Tidal Stream Turbines Subjected to Rotor Imbalance Faults*, PhD Thesis, Cardiff University, 2017.
- [30] T. Blackmore, L. Meyers, A. Bahaj, Effects of turbulence on tidal turbines: implications to performance, blade loads and condition monitoring, *Int. J. Mar. Energy* 14 (2016) 1–26.
- [31] S. Ordonez, K. Porter, C. Frost, M. Allmark, C. Johnstone, T. O'Doherty, Effects of extreme wave-current interactions on the performance of tidal stream turbines, in: 3rd Asian Wave and Tidal Energy Conference (AWTEC, 2016), 2016.
- [32] B. Christopher, *Pattern Recognition and Machine Learning*, first ed., Springer, 2006.
- [33] M.L. Stein, *Interpolation of Spatial Data: Some Theory for Kriging*, Springer Science & Business Media, 2012.